The NA48 Liquid Krypton Calorimeter

Sandro Palestini, CERN

20 January 2022

The physics program and the calorimeter

Measure the double ratio:

$$R = \frac{BR(K_L \to \pi^0\pi^0)\, BR(K_S \to \pi^+\pi^-)}{BR(K_S \to \pi^0\pi^0)\, BR(K_L \to \pi^+\pi^-)} = 1 - 6\,\mathrm{Re}(\varepsilon'/\varepsilon)$$

by counting the number of decays in two beams of K_L and K_S

Need $> 3.\,10^6$ $K_L \to \pi^0\pi^0$ for stat. error on $R < 0.1\%$ and look for cancellation of systematic effects related to differences in acceptance, efficiency, backgrounds:
(lifetimes are very different, KL decays are *rare* and are affected by background)

$c\tau_S$ = 2.67 cm
$c\tau_L$ = 15.5 m

$K_S \to \pi^+\pi^-$:	69%	$K_L \to \pi^+\pi^-$:	0.2%
$K_S \to \pi^0\pi^0$:	31%	$K_L \to \pi^0\pi^0$:	0.1%

Simultaneous data taking with both beams and both *charged* and *neutral* modes.

Control of systematics related to fiducial volume.

Backgrounds (e.g. K_L to 3 π^0) reduced to per mille level.

Beams and detector were designed for NA48

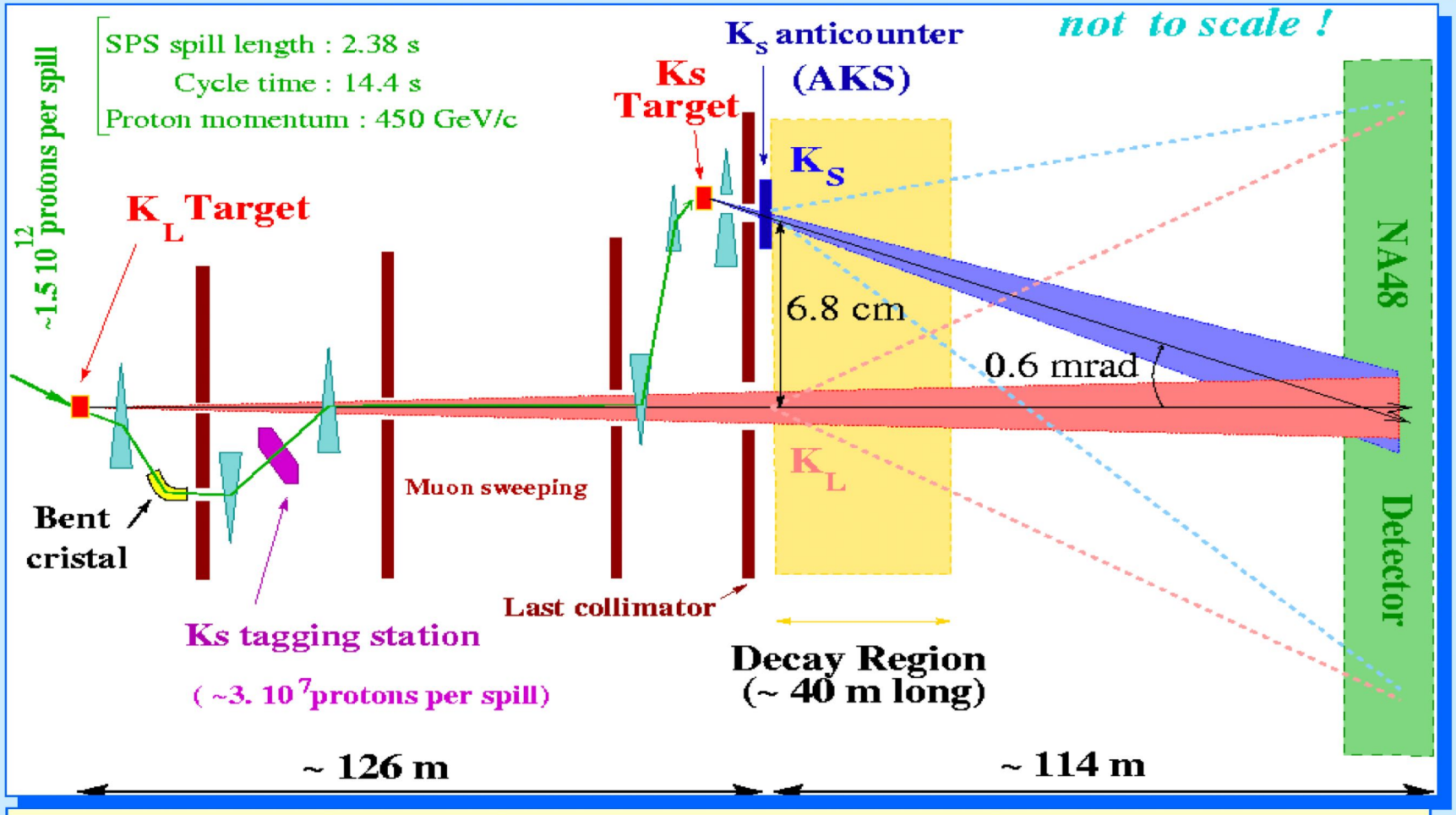

2.6 m

2 10^7 K_L per pulse
200 K_S per pulse
(2.5 s, 14.4 s cycle)

70-170 GeV momentum range used per analysis

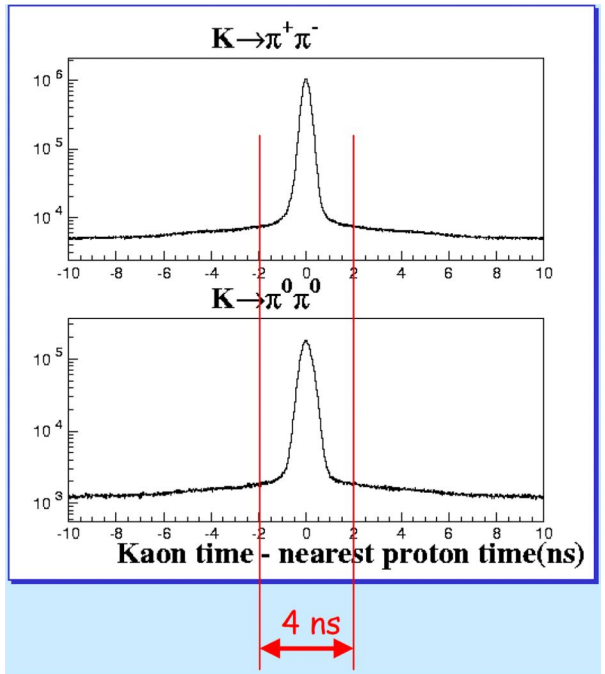

Detector and Ks tagging coincidence

NA48 Detector

- Muon veto and hadron calorimeter (background, trigger)
- Quasi homogeneous liquid krypton calorimeter to detect $\pi^0\pi^0$ events
- Scintillation hodoscope (trigger and timing $\pi^+\pi^-$)
- Magnetic spectrometer to detect $\pi^+\pi^-$ events

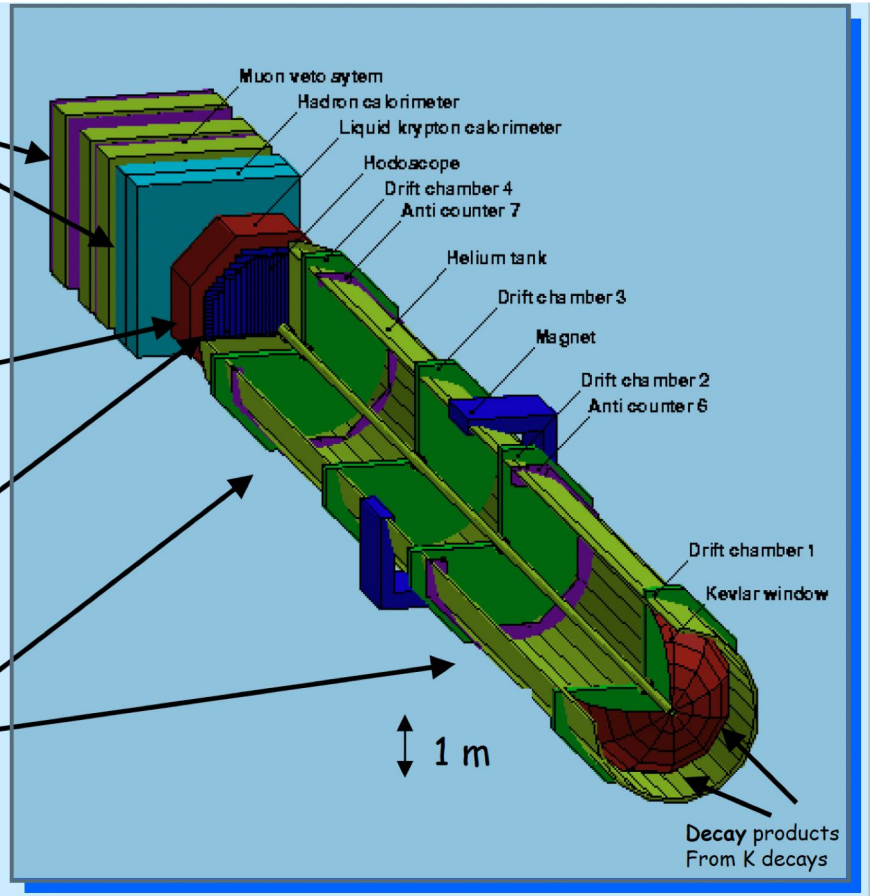

LKr readout structure before insertion in cryostat

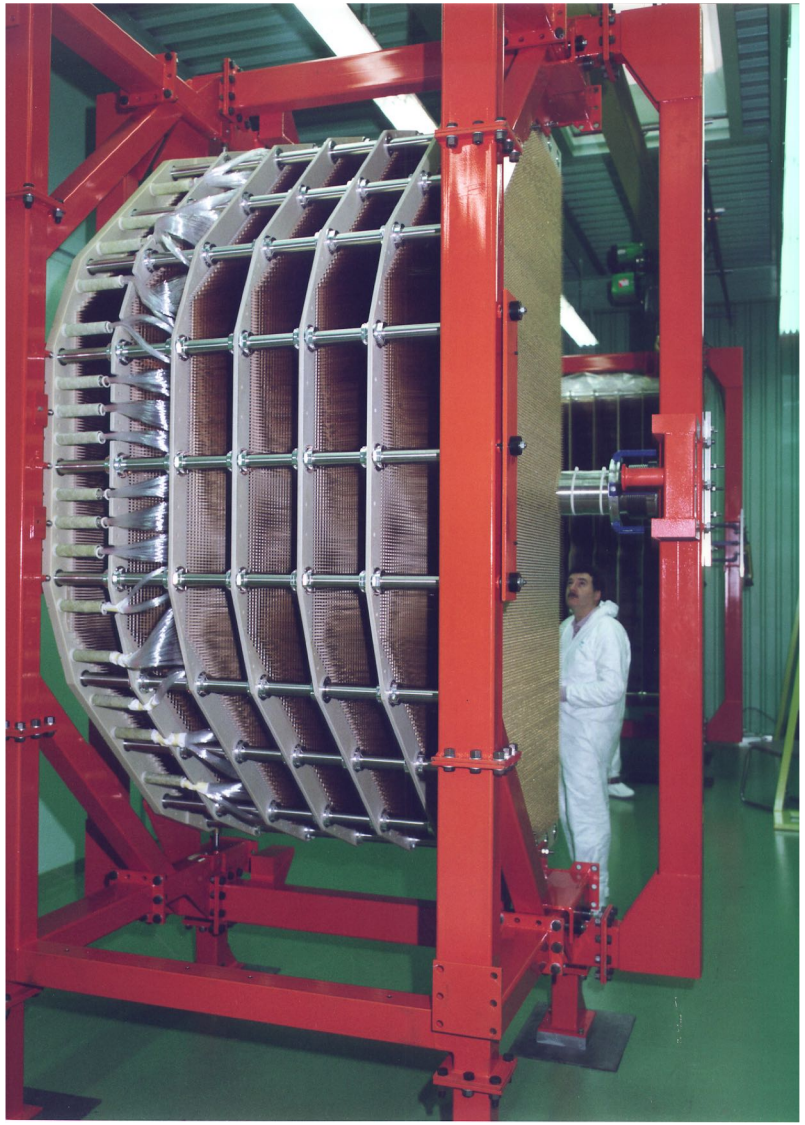

The detector was ~25 m long (downstream of the ~90 m decay tube).
The most innovative component was the e.m. calorimeter. *(biased view?)*

Calorimeter design

- The calorimeter in the previous generation ε'/ε experiment (CERN NA31) was an argon-iron sampling calorimeter
  - Longitudinally segmented
  - Readout in transverse projections
- For NA48:
  - Nearly homogeneous detector (better resolution)
  - Readout in longitudinal towers (better control of bkg., better online/offline selection and reconstruction)
  - Resolution and accuracy in reconstruction of transverse shower axis coordinates
  - Energy scale accuracy
- Stability of response lead to the choice of maintaining a noble-element liquid detector with readout of ionization charge
- Viable longitudinal and transverse dimension of showers lead to the choice of liquid krypton

Geometry of the readout structure

- Projective geometry pointing to decay region (~ 114 m upstream)
- Accordion geometry (± 48 mrad)
- Initial current read-out

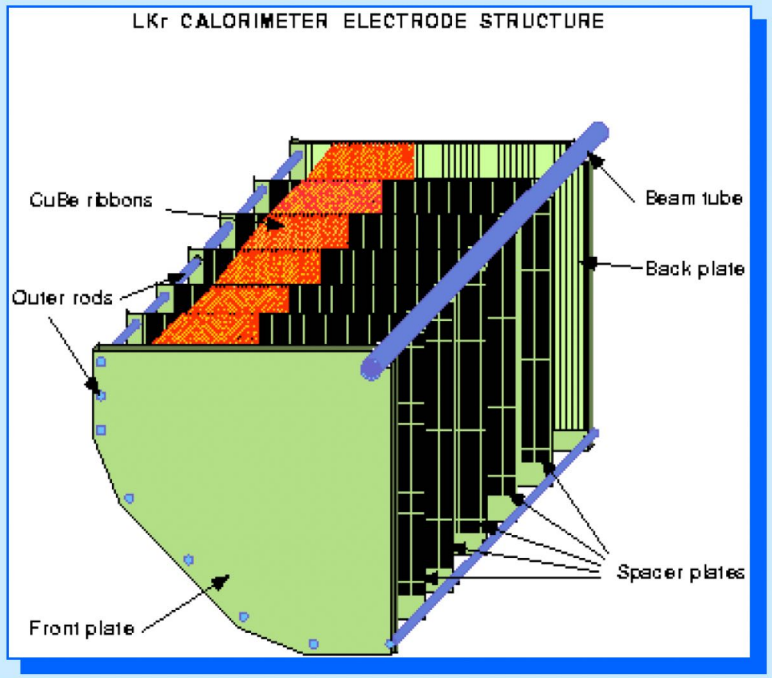

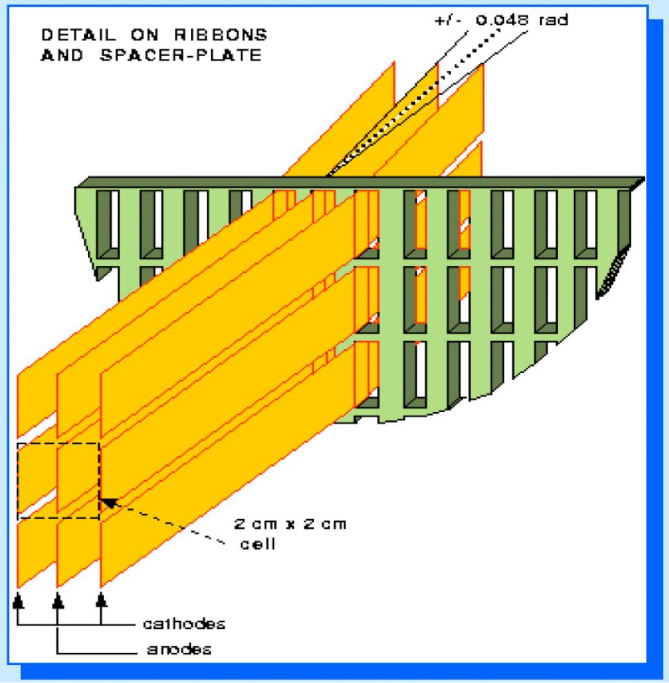

An **accordion geometry** of the readout was developed at about the same time for ATLAS, for similar reasons but with a sampling detector.

For NA48, originally this need was not obvious.
The first (small prototype) used strips etched on kapton sheets stretched between front and back plates
but this was not good enough
A design variation to the first had combs holding the the sheets flat
better …
The second prototype (and the final detector) had Cu-Be ribbons and *spacer plates* driving the readout geometry *good!*

Initial current readout

- Initial current readout to remove dependence on the distribution of the shower ionization inside the cells.
- Based on a scheme developed here, applied shaping with two differential and 4 integrating stages.
- 70 ns FWHM positive peak, undershoot about 3% amplitude, lasting 3 μs.
- Digitization at 40 MHz, 10 bits + 4 for dynamical switching for 14 bits equivalent. Digital pipeline.
- Incoherent noise 2 LSB, coherent noise 0.12 LSB, with 1 LSB = 4.2 MeV (about 120 MeV noise on a shower cluster of ~100 channels)
- 13248 readout channels.
- Electronic calibration, and data based calibration.

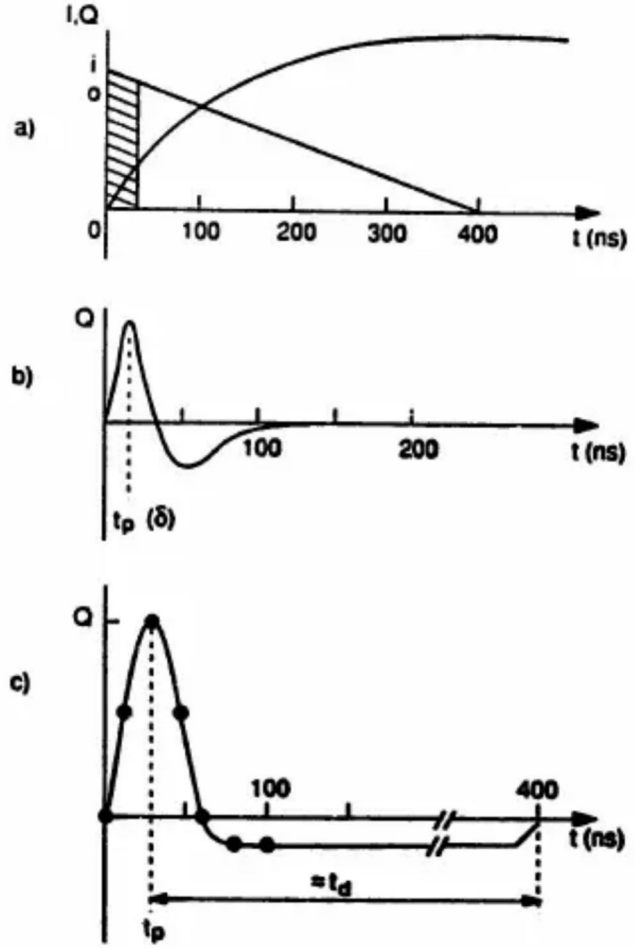

Fig. 1. (a) Drift current and integrated charge vs time for an ion chamber calorimeter. (b) Response of a bipolar shaping amplifier to a short current pulse (δ). (c) Response of a bipolar shaping amplifier to the current form shown in (a). The dots indicate where the beam crossings (every 15 ns) would appear if $t_p(\delta) = 20$ ns.

Sketch from an ATLAS paper of 1992

Uniformity of cell size (for longitudinal readout)

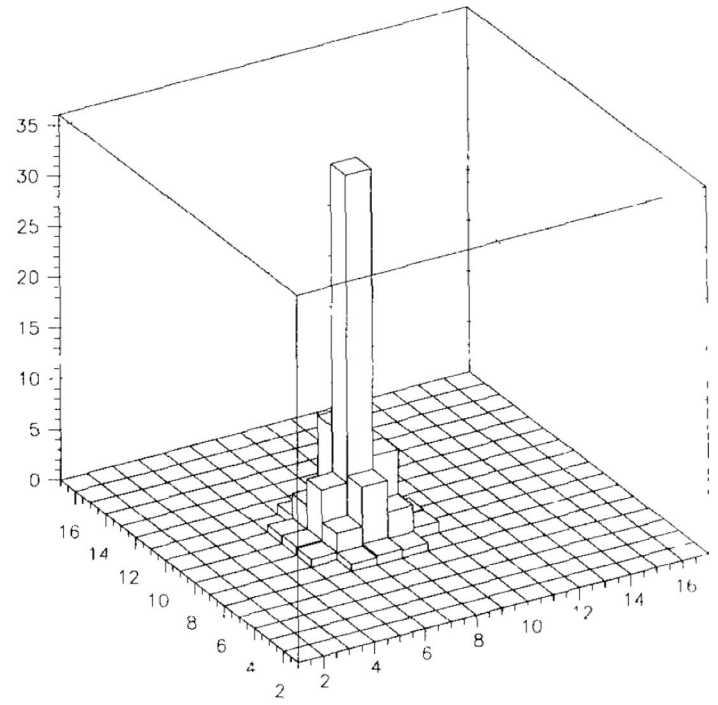

Fig. 10. Typical shower profile as measured with 120 GeV electrons.

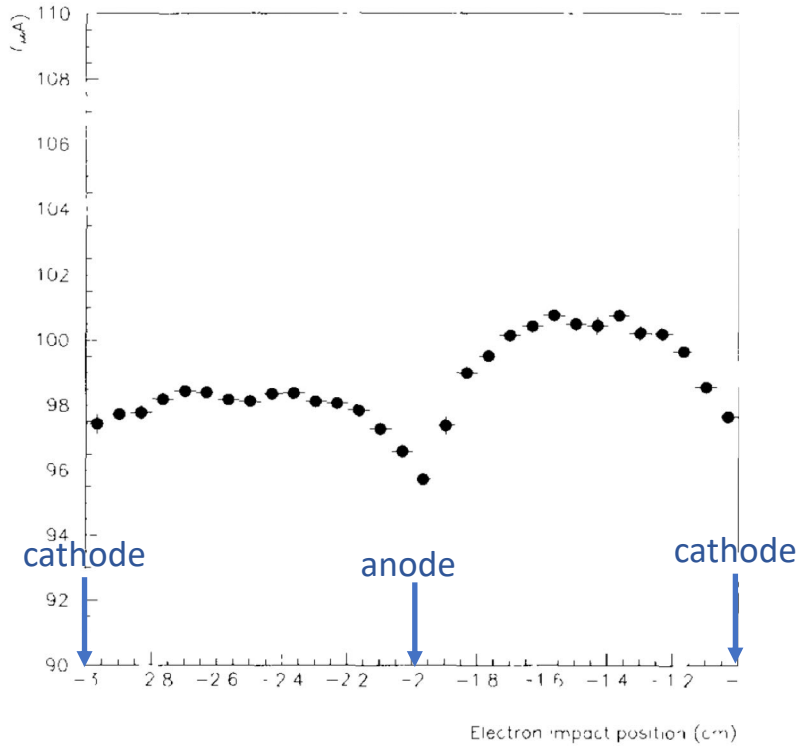

Fig. 11. Cell 76 response as a function of the electron impa position.

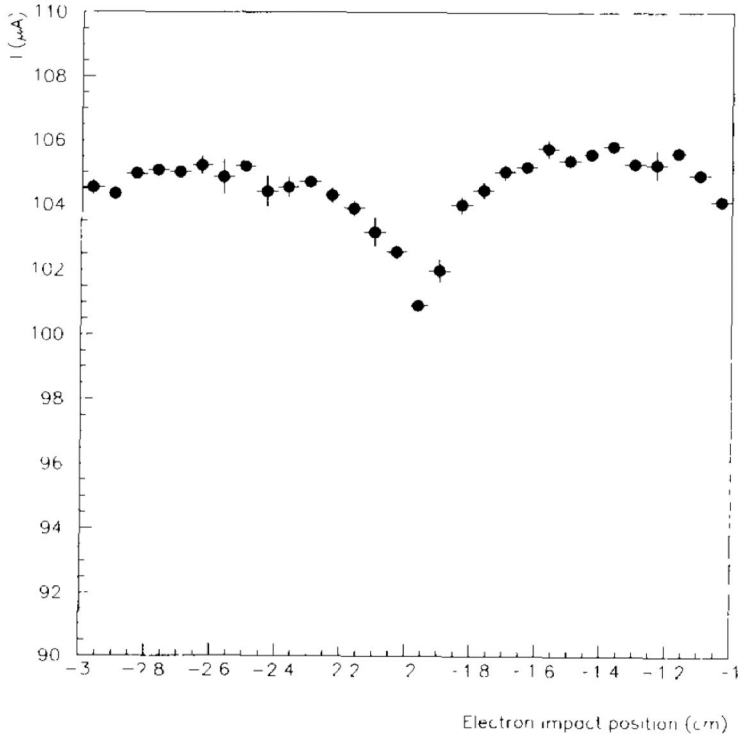

Fig. 12. Cell 76 response as a function of the electron impact position after insertion of ~~extra spacers~~. combs

LKr first prototype results: Nearly 50% of the shower energy can be collected in a single cell,
and within a cell the response depends on the position of the shower core: the finite integration time contributes to the drop in the middle. Besides, an asymmetry between the gap with in the two half-cells (about 5% in this case) generates ther asymmetry in the middle plot, substantially fixed with combs. (i = q v /d , d = gap length for infinite plate approximation)

Ribbons and spacers

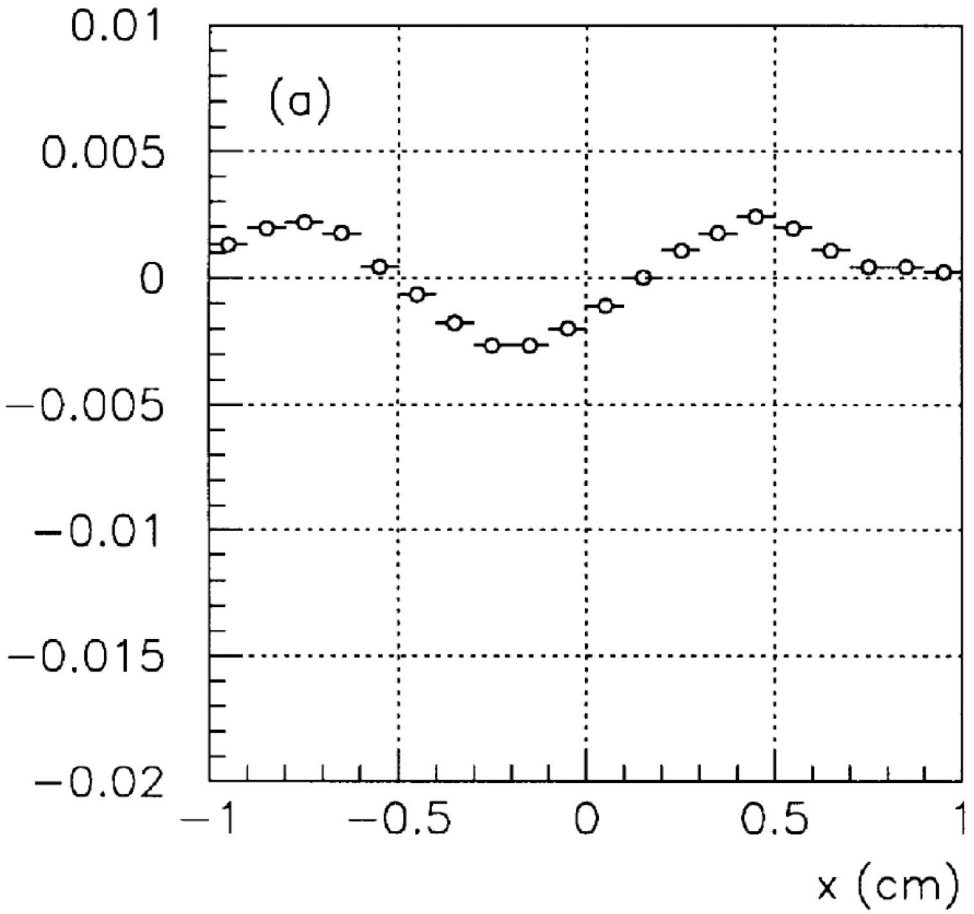

- The accordion geometry establishes an accurate gap (manufactured within 50 μm).
- There is still x dependence, for a smeared electrode effect, a few per mille.
- Transverse scale accuracy: 100 μm / m (discussed below)
- Cu-Be ribbons:
  - 40 μm thick, 18 mm wide, tensioned to 2 N
  - Integrated compliance springs

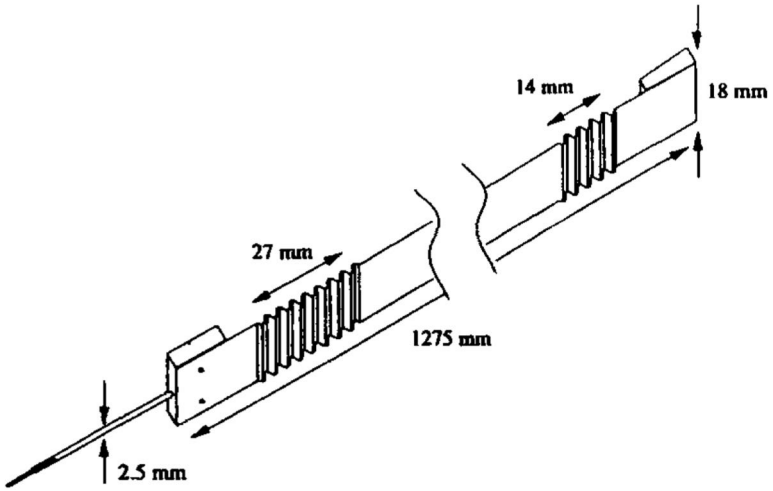

Fig. 2. Ribbon design.

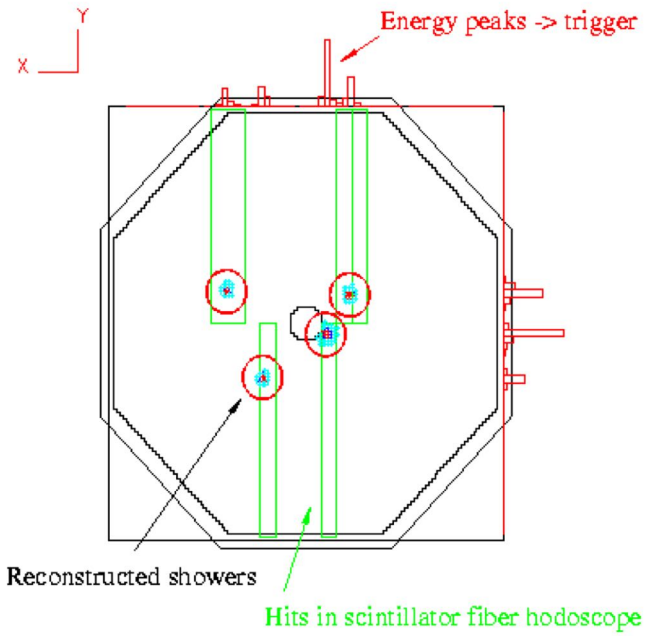

Energy and length scales

- K^0 to two π^0 events appear as 4 clusters.
- From the energy and the position measurements, and applying π^0 mass constraints, the distance between the K^0 decay point and the calorimeter is is determined. *(Think of masses as product of energies and opening angle, $m=(E_1E_2)^{0.5}\Omega$, and $\Omega \sim x/\Delta Z$)*
- Both distance and K0 energy are critical in defining the fiducial volume over which the number of decays is counted.
- The second constraint to define both scales of energy and distances was the upstream end of the K_S decay region, identified by a dedicated veto counter

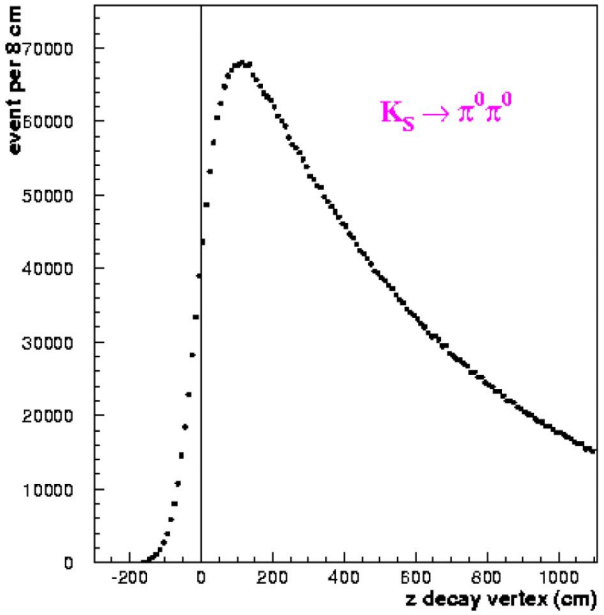

- Spectrum of reconstructed z of decay vertices, non-vetoed events. The detector is at z of about 11000 cm. The value unfolded edge (a length scale measurement) can be turned into an energy scale calibration.

  It did not vary more than 5 10^{-4} over each year of data taking.
  (K^0 and π^0 masses are known to 1/20 – 1/100 of this.)

Calorimeter performance

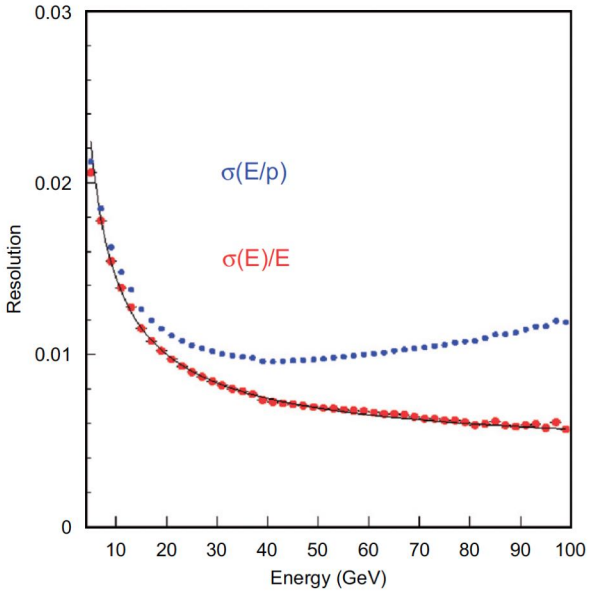

Fig. 13. Energy resolution of the calorimeter.

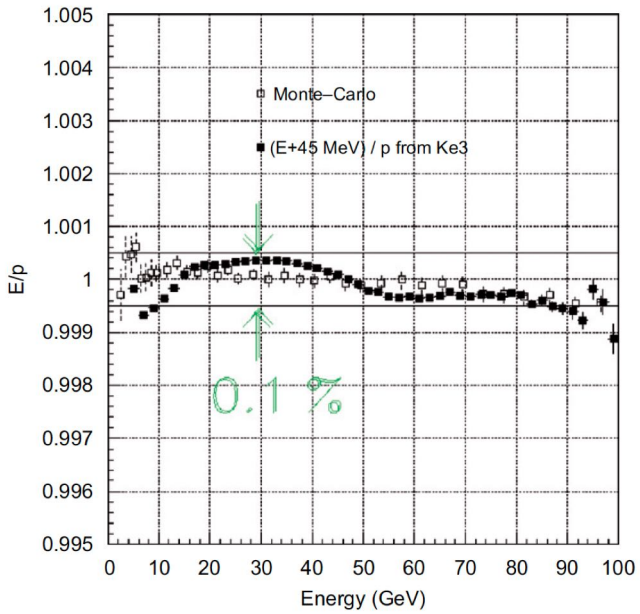

Fig. 12. Linearity of the energy response.

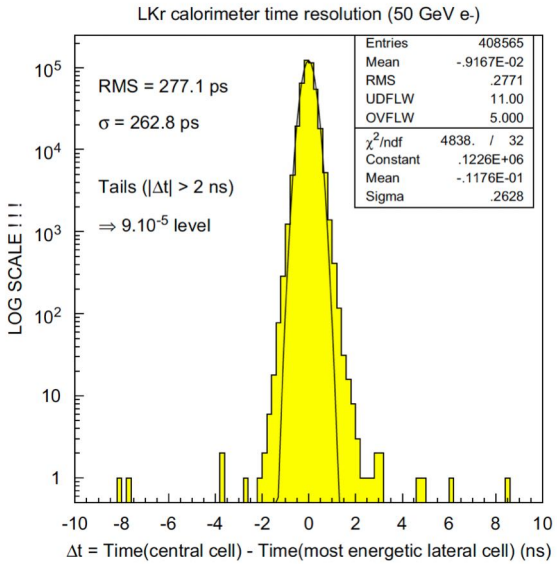

Fig. 14. Time resolution of the calorimeter.

$$\frac{\sigma_E}{E} = \frac{0.032}{\sqrt{E}} \oplus \frac{0.09}{E} \oplus 0.0042$$

$$\sigma_{X,Y} = \frac{0.42}{\sqrt{E}} \oplus 0.06 \quad \text{cm}$$

$$\sigma_t = \frac{2.5}{\sqrt{E}} . \text{ns}$$

mm

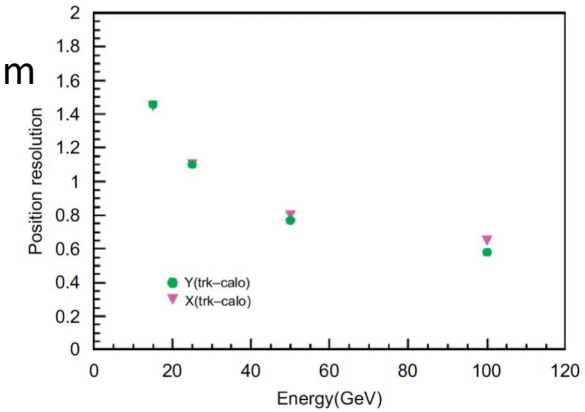

Fig. 15. Position resolution of the calorimeter.

Energy linearity and resolution, transverse position resolution obtained from dedicated electron beam, moved along a vertical band of the detector.
Time resolution also obtained from comparison of calorimeter and K_S tagger station (the latter also compared with charged hodoscope in $\pi^+\pi^-$ mode)

Special subject: space charge effects

- If the first year operation, the calorimeter was operated with 1.5 kV over the 1 cm cell, rather than the design value of 3 kV (form problems with the 3nF HV capacitors on each readout channel).
- The combination of high intensity and low voltage made the detector sensitive to space chare effects in the central region (r dependence)
  - The E field near the anode (cathode) is reduced (increased)
  - The response of the detector, in particular for the non uniformity of the x dependence of the charge amplitude, is affected (x dependence)
  - The effect is null at the beginning of each accelerator spill, establishes over 3 seconds, then is stable (and would disappear during the inter-spill interval) (t dependence)
  - The intensity near the detector center corresponded to 1500 GeV $cm^{-2}s^{-1}$, for an effective charge injection of about 150 pC $cm^{-3}s^{-1}$ (shower longitudinal extension taken into account)

Space charge -2

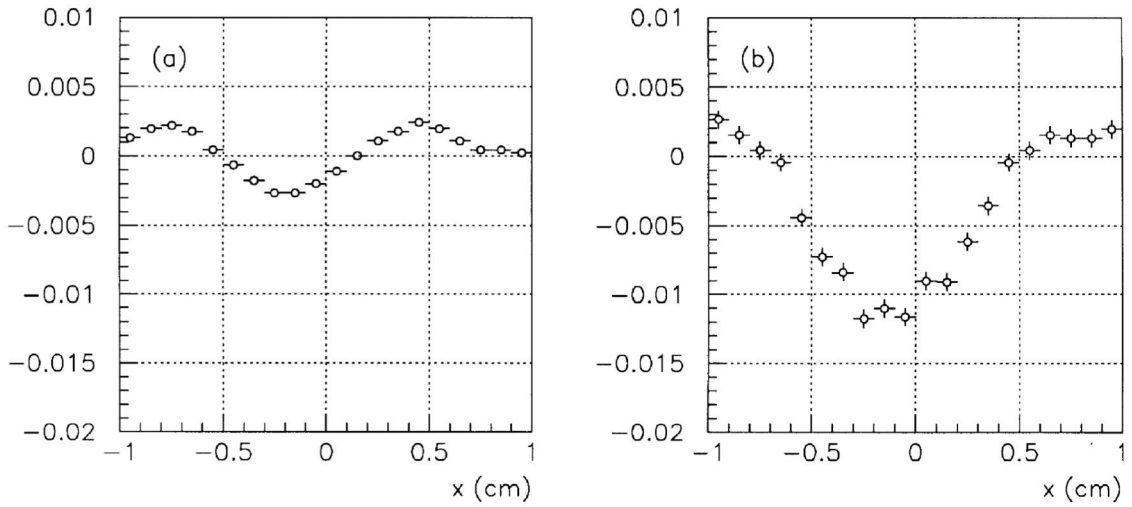

Fig. 16. Non–uniformity of detector response at low intensity (a) and at high intensity (b).

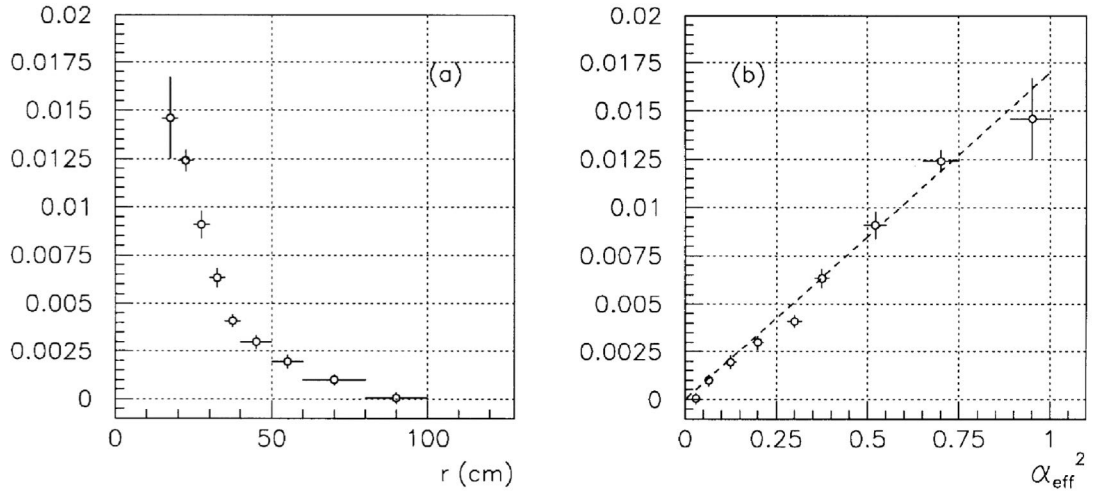

Fig. 17. Dependence of the peak-to-peak modulation of the response on the radial position (a), and on the parameter α_{eff}^2 (b).

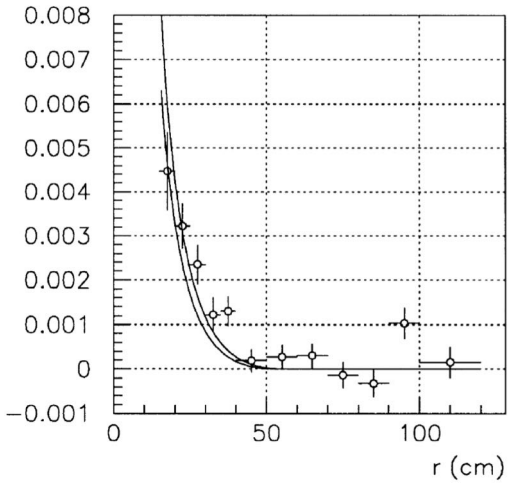

Fig. 15. Measured average reduction of response (data points) compared to the prediction.

The average drop is mainly related to non-linearity of v(E) (initial recombination can contribute)

$$\alpha = \frac{L}{E_\circ}\sqrt{\frac{K}{\epsilon\mu^+}}$$

Space charge effects are proportional to α^2, dimensionless parameter related to the ratio of space charge of positive ions, integrated across the drift gap, dividend by the surface charge on the electrodes in low intensity conditions.

Here K is the charge density injection rate, L is the gap length, μ+ is the mobility of positive ions.

Space charge 3

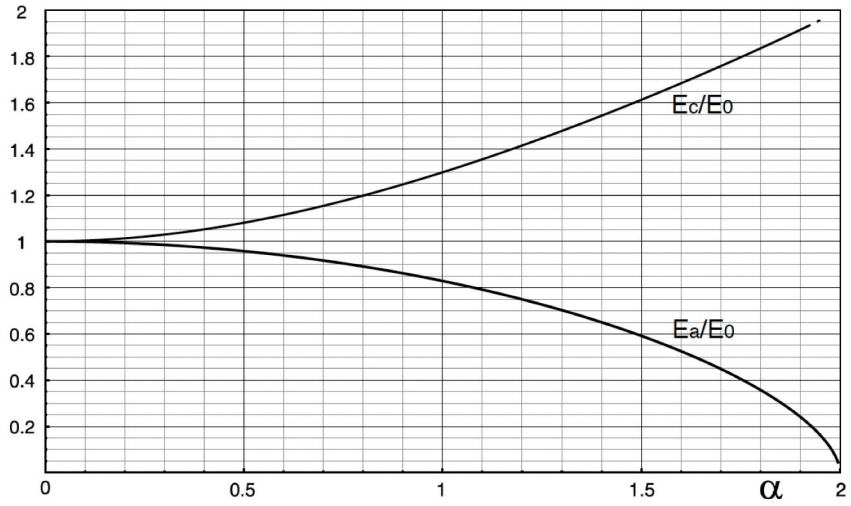

Figure 1. Normalized electric field at the anode E_a/E_o and cathode E_c/E_o as a function of the dimensionless parameter α. Reproduced from reference [5].

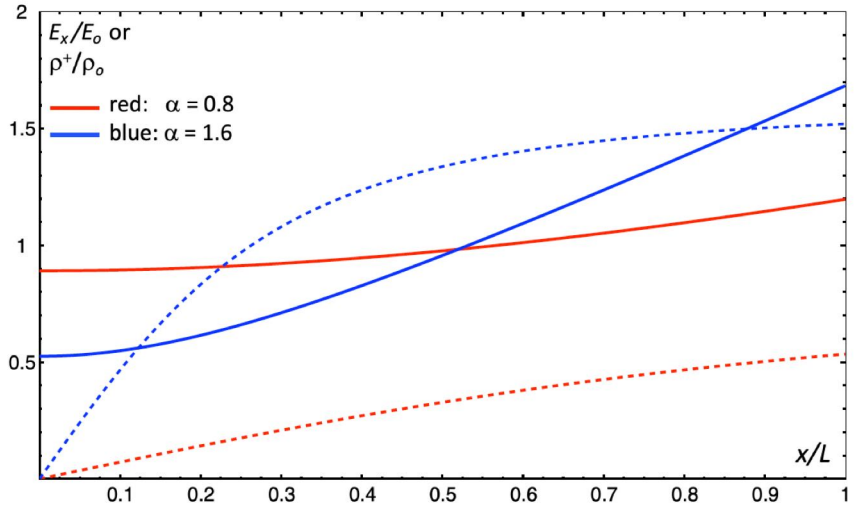

Figure 2. Electric field (continuous lines) and charge density (dashed line) behavior for $\alpha = 0.8$ (red) and $\alpha = 1.6$ (blue). The horizontal axis is the drift coordinate divided by the gap length (x/L), with $x = 0\,(1)$ at the anode (cathode). The electric field is in units of $E_o = V_o/L$, and the charge density in units of $\rho_o = \epsilon E_o/L$. Reproduced from reference [6].

Basic model of space chare effects (one dimensional, E-dependence of recombination ignored), developed at the time of first operation of the NA48 calorimeter.

Krypton natural radioactivity

- Relevant topic, because of ^{85}Kr beta decay, at about 500 Bq/cm^3, with endpoint at 670 keV.
- This was not relevant for NA48, because it did not introduce a significant noise, in the ~50 liter of shower cluster, over the short initial current integration time

Remarks concerning the subject of these meetings

- Scintillation light: we were aware of the possibility of exploiting it, as in LAr TPC, but it appeared not needed in NA48 calorimetry (difficult to maintain tower read out, timing response sufficiently fast).

- Combined scintillation and charge readout in liquid krypton TPC is very relevant (timing, triggering …)

- Charge readout on PCB boards like in the DUNE far detector 2 (Vertical Drift) proposal? Maybe on pixels rather than strips?

- Photon detector behind the faraday cage elements?

- Impact of krypton radioactivity?

Some references

NA48 beamline and detector: V. Fanti et al., NIM A 574(2007) 433-471

Initial current readout, ATLAS calorimeter: B. Aubert et al., NIN A 315 (1992) 285-293

Space charge in the NA48 calorimeter (basic model): S. Palestini at al., NIM A 421 (1999) 75-89